Trace metals dispersion from 1000 years of mining activity in the northern French Alps

Estelle Camizuli, Magali Rossi, Dominique Gasquet

Trace metals dispersion from 1000 years of mining activity in the northern French Alps

Estelle Camizuli[a], Magali Rossi[a,*], Dominique Gasquet[a]

[a]UMR 5204 EDYTEM, Université Savoie Mont Blanc – CNRS, 73376 Le Bourget-du-Lac cedex, France
[*]Corresponding author, email address: magali.rossi@univ-smb.fr

Acknowledgements

The authors are grateful to the University of Savoie Mont-Blanc for funding the one-year post-doctoral fellowship for Estelle Camizuli and for funding the TraMines research project, directed by Magali Rossi and Marie Forget (EDYTEM laboratory). This study was also funded by the French national research program EC2CO-Biohefect of the CNRS (TRACES project, grant number 183446). The authors warmly thank Robert Durand for his knowledge concerning local mines and his personal data and particularly Bruno Tourlière, in the BRGM, for providing the sediment database used for this study.

Abstract

This paper investigates the long-term dispersal of trace metals and their impact on the environment long after mine closure in the French Alps. Three statistical methods derived from modern mining (Exploratory Data Analysis, fractals and Sediment Quality Index) were applied to geochemical analyses of streambed sediments to produce mineral prospectivity maps. About 5% of the samples have a poor or marginal quality and may have an effect on biota. Positive anomalies are either related to the geological background (lithology, major tectonic contacts) or to ancient mining sites. The local impact of former mining was investigated on a medieval Pb-Ag district (Brandes; Pb_{max} ~ 8000 $mg.kg^{-1}$), a small district mined during the 17th-19th c. (Peisey-Nancroix; Pb_{max} = 583 $mg.kg^{-1}$), and a major modern Pb-Ag mine (Macôt-La Plagne; Pb_{max} ~ 3200 $mg.kg^{-1}$).The mining heritage is still traceable in the northern French Alps. The anomalies observed at local scale are related to the volume of extracted ore rather than to the timing and duration of mining, suggesting that old mining sites still release trace metals over centuries and up to a thousand years. The statistical methods used provide a strong tool for archaeological prospection and environmental studies.

Keywords: Streambed sediments, Trace metal anomalies, Ancient mines, northern French Alps, Geostatistical methods.

1. Introduction

High trace metal (TM) concentrations in the environment may result from anthropogenic activity, and/or from natural weathering of metal-rich rocks and ore bodies. In the case of mining, both natural and anthropogenic factors are involved as mineral deposits correspond to natural positive TM anomaly, while their exploitation may considerably extend metal dispersal (MacKenzie and Pulford, 2002; Camizuli et al., 2014a; Courtin-Nomade et al., 2016; McConnell et al., 2018). Trace metals contamination around abandoned mines has been intensively investigated in soils (Ettler, 2016; Egli et al., 2017), in streambed or stream sediments (Byrne et al., 2012; Ciszewski et al., 2012; Resongles et al., 2014; Gbolo and Lopez, 2015; El Azhari et al., 2016; Potra et al., 2017; and references therein) and in vegetation (Antoniadis et al., 2017; Debén et al., 2017; Madejón et al., 2018; Schreck et al., 2020). Streambed sediments record the composite erosion products of geological formations in a catchment area, including ore and mine waste deposits located upstream (Hudson-Edwards, 2003). Therefore, they are a relevant tool to study the spatial dispersion of TMs in the environment, which can be useful for mining exploration, environmental studies and archeological investigations (Lapworth et al., 2012; Camizuli et al., 2014b; Monna et al., 2014; Kirkwood et al., 2016; Darwish, 2017; Gonçalves et al., 2017; Parsa et al., 2017; Yousefi and Nykänen, 2017; Zuluaga et al., 2017).

Most literature based on streambed sediment analyses focuses on modern mining and mines that were closed since the 1970s or during the 20th century (Casiot et al., 2009; Ferreira da Silva et al., 2009; Ciszewski et al., 2012; El Azhari et al., 2016). There are less studies focusing on mines that closed during the 19th century or earlier (Lecce and Pavlowsky, 2014; Horak and Hejcman, 2016; Kossoff et al., 2016; Mariet et al., 2017). Assessment of TMs dispersal in mining areas that were mined during Middle Ages or Antiquity are generally based on sediment cores that record primary mobilization of TMs (Elbaz-Poulichet et al., 2011), or on TMs dispersal in soils (Baron et al., 2006; Mariet et al.,

2016; Camizuli et al., 2018), when not based on atmospheric fluxes and TM deposition in ice or lake sediments (Rosman et al., 1997; West et al., 1997; Arnaud et al., 2005; Giguet-Covex et al., 2011). Rather scarce studies investigate long-term (i.e., from a hundred years to the Middle Ages or Antiquity) TMs dispersal from streambed sediment data (Garcia-Ordiales et al., 2014; Monna et al., 2014). Persistence of trace metals in streambed sediments may reach potentially toxic levels for biota over time (Camizuli et al., 2014b; Garcia-Ordiales et al., 2014; Lecce and Pavlowsky, 2014; Beane et al., 2016; Gutiérrez et al., 2016; Elbaz-Poulichet et al., 2017; Camizuli et al., 2018).

This paper investigates trace metals dispersal in the northern French Alps, where hundreds of small Fe, Cu, Pb-Zn and other metal deposits (Meloux, 1975; Durand, 2005) have been mined from the Bronze Age to the 20th century (Schibler et al., 2011; Moulin et al., 2012; Py et al., 2014). Anthropogenic lead records in high-altitude lake sediments (Arnaud et al., 2005; Giguet-Covex et al., 2011) and archeological and historical investigations (Meloux, 1975; Bailly-Maître, 2019) indicate peak activity during the Middle Ages and the 19th century. Apart from Macôt-La Plagne and St-Georges d'Hurtières mines, which closed in the 1970s and the 1930s respectively, mining activity essentially stopped in mid-19th century or during the Middle Ages. Therefore, the northern French Alps is a good area to investigate the long-term dispersal of trace metals into the environment resulting from mining-activity, over several centuries. Several statistical methods derived from modern mining prospecting and ecological management plan (Garcia-Ordiales et al., 2014; Monna et al., 2014; Afzal et al., 2016; Agharezaei and Hezarkhani, 2016; Hoang and Nguyen, 2016; Mortazavi and Saberinasab, 2017) were applied to the streambed sediment database provided by the *Bureau de Recherches Géologiques et Minières* (BRGM; French Geological Survey). Regional prospectivity maps were produced using Exploratory Data Analysis (EDA) and a fractal-based model to highlight As, Cu, Ni, Pb, and Zn anomalies. Sediment Quality Index (SQI, Marvin et al., 2004) was also computed from seven TM concentrations (As, Cd, Cr, Cu, Ni, Pb, and Zn) to assess the overall quality of streambed sediments based on eco-toxicological thresholds. In order to investigate the local impact of ancient mining activity, this paper focuses on three major Pb-Ag mining districts that were mined at different historical periods from the Middle Ages to Modern Times: (i) Brandes, which was an important medieval Pb-Ag exploitation, (ii) Peisey-Nancroix, which was mined during the 17th-19th c. AD, and (iii) Macôt-La Plagne, which was a huge modern Pb-Ag mining area before becoming a major ski resort in the 1970s (Durand, 2005, 2010). In the French Alps, silver was mined since at least the Middle Ages as it was used for mint (Bailly-Maître, 1989, 2019). Pb-Ag mines are thus good candidates to study the local impact of past mining activity from streambed sediments analyses considering Pb is a stable element that remains for a long time in the environment, and is associated with other TMs such as arsenic, antimony or copper.

2. Geological and historical contexts

2.1. Geological setting

This study focuses on the northern French Alps, in an area of c. 4700 km² (Fig. 1a), with the altitude ranging from 300 m a.s.l. up to more than 3000 m a.s.l., resulting in a complex hydrographical network.

The current structure of the Alpine belt reflects its complex history. The external Alps represent the old European margin whereas the internal Alps correspond to the old Apulian

margin. The internal and external Alps, separated each other by the major Penninic Front, consist of magmatic and metamorphic rocks formed during the Variscan orogeny that were exhumed during the Alpine collision, and extruded into their Mesozoic sedimentary cover during the Alpine orogeny (Coward et al., 1989; Agard and Lemoine, 2003; Marthaler, 2005). The metamorphic Variscan basement is mainly composed of various gneisses, micaschists, migmatites and mafic rocks (amphibolites and metagabbros) intruded by Variscan and late-Variscan granitoids. These rocks essentially crop out in the external crystalline massifs (Ecrins-Pelvoux, Belledonne and Lauzière) of the external Alps. In the internal Alps, Variscan micaschists, Carboniferous schists and Cretaceous schists are abundant. The Mesozoic sedimentary cover is mainly composed of Triassic dolomites (internal Alps) and Jurassic and Cretaceous limestones and marls (external Alps). These lithologies correspond to the carbonates in Figure 1. Eocene flysches are the most abundant detrital rocks. Superficial deposits (Quaternary tills and alluviums) are found in the main valleys.

The complex Variscan and Alpine orogeneses were characterized by major fluid flows that were locally responsible for metal concentrations that have been mined since Antiquity (Py et al., 2014). However, the distribution and size of ore deposits is very heterogeneous depending on the geological setting. The Eastern Alps hosted some world class Fe-Cu-Sn deposits that have been mined since the Bronze Age (Schibler et al., 2011); some being still operated as open pits. On the opposite, the French Alps are characterized by numerous and disseminated small size ore deposits; about 350 ore deposits have been reported by the BRGM, but this number has been reassessed by Durand (2005, 2010).

Base-metal deposits (Fe, Cu, Pb-Zn-Ag) are the most common in the French Alps. With the exception of some sedimentary iron ores, most deposits occur as vein-type and stratiform mineralization that were operated underground. The distribution and size of ore deposits are clearly depending on the geological setting. Most ore deposits are located in the external Alps, in the External Crystalline Massifs and in the Permo-Triassic sedimentary formations. Some ore deposits are also located in the internal zone and are mainly hosted in the carboniferous schists (Fig. 1a; Meloux, 1975; Rossi and Gasquet, 2014; Gasquet and Rossi, 2015).

2.2. Mining activity in the northern French Alps

The mining industry was quite important in the French Alps. Since the Bronze Age, mining activity contributed to human settlement and economic development (Py et al., 2014). If many alpine mines were operated since Antiquity, mining activity reached its maximum during the Middle Ages and the 19th century, as evidenced by Pb records in lake sediments and peat bogs (Arnaud et al., 2005; Giguet-Covex et al., 2011; Py et al., 2014). The activity started to decline at the end of the 19th century (Gasquet and Rossi, 2015) due to the discovery of giant ore deposits worldwide. Metallurgical industries developed since the 19th century, due to the mining and processing industry and to the development of hydro-electricity. These industries are still in activity in the alpine valleys.

In the study area, 137 mining sites have been reported by the BRGM (Fig. 1b). Data and complementary information were freely available online at http://sigminesfrance.brgm.fr (last accessed 19 July 2019; now moved to http://infoterre.brgm.fr, *Gisements, gîtes et indices* and *Mines-Substances principales* databases). Most mines were small-scale underground exploitations, sometimes located above 1500 m, a.s.l. A few districts were more important, such as the St-Georges-d'Hurtières district which provided 1.5 Mt of siderite and more than 10 000 t of chalcopyrite between the Middle Ages and the 20th century.

This paper focuses on trace metals dispersal around the three main Pb-Zn-Ag districts of the northern French Alps that were mined at different time periods from the Middle Ages to Modern Times. The *Macôt-La Plagne* mine, located at 1800 m a.s.l., has been one of the most important Pb-Ag mine in France: 126 600 t Pb and 350 t Ag were extracted from 1810 to 1973 (Meloux, 1975). Mining activity was stopped due to the discovery of huge deposits worldwide making extraction no more profitable, and to the development of a major ski resort at La Plagne. Historical and archaeological records indicate that Pb-Ag may have been episodically extracted in Macôt-La Plagne since Roman Period (Gimard, 1987). The Pb-Ag mine of *Peisey-Nancroix*, located ~10 km east of Macôt-La Plagne at 1500 m a.s.l., was mined from 1644 to 1865, with a peak activity in the 18th century (Nicolas, 1978): 22 000 t of Pb and 53 t of Ag were extracted during this period (Meloux, 1975). Episodic mining activity occurred during the Middle Ages (Durand, 2010). Opposite to Macôt-La Plagne, the site has been unmodified since mine closure in 1865 and waste deposits (tailings, slags and washing residues) have been preserved on site. The *Brandes* (Huez, Oisans) district, located at high altitude (between 1800 and 2700 m a.s.l) was the most important medieval Pb-Ag exploitation in the French Alps. Archeological surveys show rational mining activity (metallurgical wastes, workshops, hydraulic equipments) from the 11th to the 17th centuries (Bailly-Maître, 1989, 2019). There is no estimation of the extracted ore volume since the 11th century, but 900 000 tons of dumps (mainly barite) are bordering the Brandes plateau (pers. com. M.Ch. Bailly-Maître).

3. Materials and Methods

3.1. Geochemical data

In the study area, the BRGM collected 6892 samples of streambed sediments (Fig. 1c). The analyses were undertaken during the 1980s through an inventory of mineral substances at the national scale (Lambert, 2005). Sediments were sieved at 125 µm, dried, and analyzed after a near-total dissolution for As, Cd, Cr, Cu, Ni, Pb, and Zn by Direct-Current Plasma spectroscopy. Data and complementary information were freely available online at http://sigminesfrance.brgm.fr (now moved to http://infoterre.brgm.fr, *Géochimie-Inventaire Minier*). Less than 15 % of the dataset display values below the limit of detection (LOD) for all elements except Cd, which display 93% data below LOD (Table 1). These data contain useful information and were thus substituted by a value of 75 % of the limit of detection as recommended in environmental sciences (Baxter et al., 2000; Helsel, 2012).

A focus on the three Pb-Ag mining districts was realized at the same spatial scale (1:40 000, ~36 km²) from the BRGM dataset: 64 samples are available in Brandes, 50 samples in Peisey-Nancroix, and 74 samples in Macôt-La Plagne. At this scale, more samples would be required in order to provide better statistical results.

3.2. Data processing and statistical treatment

The Quantum GIS free software was used for mapping (QGIS Development Team, 2017), and the rgr, akima, segmented, and StatDA packages of the R free software (version 3.3.2--Sincere Pumpkin Patch) were used for statistical treatment (R Core Team, 2017).

3.3. Single-element approaches

193 *3.3.1. Exploratory data analysis*
194
195 Exploratory Data Analysis (EDA) is a robust method for the study of patterns and the
196 identification of outliers (Reimann et al., 2008; Carranza, 2011), using descriptive statistics
197 and graphical tools (Tukey, 1977). EDA-based mapping allows subdivision of the dataset
198 into seven categories: (i) far low outliers, (ii) near low outliers, (iii) low background, (iv)
199 background, (v) high background, (vi) near high outliers, and (vii) and far high outliers (see
200 detailed methodology in Camizuli and Carranza, 2018).
201 As geochemical analyses may vary according to the lithological units, a
202 transformation procedure was applied to the dataset before computing threshold by EDA
203 (see Pb in Fig. 2a), using the following equation (Bonham-Carter and Goodfellow, 1986;
204 Carranza and Hale, 1997; Yusta et al., 1998):
205
206 $Z_{i,j} = (X_{i,j}-med_{i,j})/MAD_{i,j}$ (1)
207
208 where $Z_{i,j}$ represents the standardized data value for the element i of the lithology j. The
209 MAD - Median Absolute Deviation - is equivalent to the standard deviation (Tukey, 1977),
210 and is defined as $MAD_{i,j} = med[|X_{i,j}-med_{i,j}|]$, where med represents the median. In the study
211 region, the complex geological units have been simplified into eight lithological categories: (i)
212 granitoids (n=635), (ii) superficial deposits (n=160), (iii) detrital rocks (n=239), (iv)
213 carbonates (n=2700), (v) gneisses (n=286), (vi) schists (n=2267), (vii) mafic rocks (n=351),
214 and (viii) migmatites (n=254).
215
216 With such a transformation, however, half the values are negative and cannot be log-
217 transformed, as recommended by Reimann et al. (2008) for strongly skewed data.
218 Therefore, the following transformation was performed to make all values greater or equal to
219 1 (see Pb in Fig. 2b):
220
221 $z_{i,j} = 1 + Z_{i,j} - min(Z_{i,j})$ (2)
222
223 Once the data became comparable, six Tukey thresholds were computed, for each
224 considered element, defining the seven anomalies categories mentioned above for EDA
225 mapping. The thresholds were calculated using the map.eda7 function of the rgr package
226 (Garrett, 2013, 2016), supplementing the R software (R Core Team, 2017).
227
228 *3.3.2. Fractal-based model*
229
230 The fractal approach consists in an improvement with respect to the empirically-driven EDA-
231 method, as it integrates the spatial correlation of geochemical data and the scale-
232 independent features of geochemical landscapes (i.e., objects presenting a fractal
233 dimension; Carranza, 2009). Fractal models are based on the geochemical distribution
234 patterns resulting from numerous geological processes that took place at different rates and
235 different temporal and geographical scales (Zuo and Wang, 2016).
236 The concentration-area plot, developed by Cheng et al. (1994), assesses whether
237 the data are spatially multi-fractal, which is useful to determine the occurrence of multiple
238 populations that are spatially dependent in the dataset. It can be used to determine the
239 practical limits, upper or lower bounds, of the influence of the biogeochemical processes
240 behind the spatial distribution of the data.

The caplot function of the rgr package (Garrett, 2013, 2016), supplementing the R software (R Core Team, 2017) was used to compute the concentration-area plot (see detailed methodology in Monna et al., 2014). The breakpoints (thresholds) of the straight lines, fitted by ordinary least square regression, were estimated through the segmented function of the segmented package. This function allows to express regression model with segmented relationships. The slope, intercept and adjusted-R-squared have been computed for each subset.

3.4. Multi-element approach: sediment quality index

The Sediment Quality Index (SQI) developed by the Canadian Council of Ministers of the Environment (CCME, 2002) and modified later by Marvin et al. (2004), was chosen to describe the overall quality of the streambed sediments. Originally, the guideline values, used by the Canadian government, were the Probable Effect Levels (PELs, Marvin et al., 2004). However, MacDonald et al. (2000) have developed consensus-based Sediment Quality Guidelines (SQGs) for several contaminants, including a Threshold Effect Concentration (TEC) and a Probable Effect Concentration (PEC). For this study, as there is a lack of clear directives in France, and even in the European Union (Besten et al., 2003), the PEC values of As, Cd, Cr, Cu, Ni, Pb, and Zn (Table 1) were selected as reference values to calculate the SQIs. These values correspond to the levels above which harmful effects on sediment-dwelling organisms are expected to occur frequently (MacDonald et al., 2000). An index score was computed for each sample, taking into account the number of variables exceeding the guideline values, as well as the magnitude of their respective excess. Calculation of SQIs is detailed in Camizuli et al. (2014b). Final SQIs are expressed as a percentage, thus permitting inter-sample comparisons. To facilitate data representation, the five SQI categories of sediment quality defined by Marvin et al. (2004) have been used: poor quality (0-45), marginal quality (45-60), fair quality (60-80), good quality (80-95), and excellent quality (95-100).

4. Results

4.1. Geochemical data

Maximum chemical element concentrations in streambed sediments vary widely and can reach extremely high values: 1076 $mg.kg^{-1}$ for As, 45 $mg.kg^{-1}$ for Cd, 1700 $mg.kg^{-1}$ for Cr, 1530 $mg.kg^{-1}$ for Cu, 1571 $mg.kg^{-1}$ for Ni, 8900 $mg.kg^{-1}$ for Pb, and 8190 $mg.kg^{-1}$ for Zn. Except for Cd, which displays 93% data below LOD, the other elements exhibit asymmetric distributions, which tend to be more compatible with normal law once log10-transformed, as shown by changes in skewness (Table 1).

4.2. Single-element approaches

4.2.1. Exploratory Data Analysis

The percentage of data per EDA category is comparable for each element, with 49-50 % of the sample (n ~ 3400 samples) in the background category (Table 2). The distribution in the high outlier categories (near and far) vary according to the elements. Most geochemical

anomalies are related to arsenic, then to lead and zinc, and finally to copper, which presents the smallest anomaly number.

Anomalies can be very localized; their spatial distribution is different for each element (Fig. 3a, Fig. S1a). 5.2% of streambed sediments present a high As anomaly. Most As anomalies are geologically controlled, as evidenced (i) from a cluster of more than 200 samples in the high outliers categories localized in the *Série Satinée* micaschists around Albertville, and (ii) from the alignment of anomalies along the major tectonic structures on the SE side of the External Crystalline Massifs (contact of the Variscan basement and the Mesozoic sedimentary cover). Some other anomalies, which are less spread, are associated with former mining activities (e.g. Chalanches mine) or to the occurrence of unmined hydrothermal veins.

Lead and zinc anomalies display a similar spatial pattern, which is more heterogeneous than for arsenic, and well distributed all over the study area, suggesting no lithological control. 5.1% of streambed sediments present a high Pb anomaly. Opposite to As, Pb anomalies are mainly related to former mining activity (e.g., Macôt-La Plagne and Peisey-Nancroix district; Brandes district; Rocheray district near St-Jean de Maurienne; Chalanches district, etc.). However, a good correlation is observed between Pb anomalies and major tectonic structures or unmined hydrothermal veins. Nickel anomalies are less numerous (3%) and correspond to several limited clusters that are directly related to ultramafic or mafic rocks in the Belledonne, Grandes Rousses and Vanoise massifs.

Copper anomalies (2.3%) are mostly dispersed within the External Crystalline Massifs (Grandes-Rousses, Belledonne, Beaufortain). Even though copper mines and deposits are located in this domain (e.g., St-Georges d'Hurtières), there is no clear relationship between Cu anomalies and mining.

4.2.2. Fractal-based model

With the fractal approach, the number of samples presenting a high or very high anomaly ranges between 0.5 % (n=33) for Ni and 2 % (n=143) for As (Table 3). This method discriminates few clusters, but the spatial distribution and the intensity of the anomalies are different for each element (Fig. 3b, Fig. S1b).

The distribution of As anomalies is similar to that of EDA ones: the lithological control of the *Série Satinée* micaschists remains evident (Albertville area; ~ 100 samples out of 143), but clusters are highlighted along the internal contact of the ECM, which are related to the occurrence of Au veins in the Glandon and Madeleine passes.

Lead and zinc anomalies display similar pattern; they are mainly localized in the vicinity of former Pb-Zn-Ag mines. Nickel anomalies are very rare (0.5% of samples) and localized downstream mafic rocks, providing evidence of a strong lithological control. Copper anomalies are scattered in the ECM displaying a pattern similar to EDA one, controlled essentially by geology but not by former mining activity.

4.3. Multi-element approach

More than 60 % of the 6892 samples belong to the good or excellent SQI categories (Table 4). This percentage reaches ~95 % if the fair SQI category is included. Several clusters with low SQIs (5 % of the samples) can be distinguished in Fig. 4. The largest cluster is located in around Albertville, in the *Série Satinée* micaschists of Beaufortain and Lauzière. Another striking cluster follows the Arc river on approximately 7 km near Bonneval-sur-Arc, in the

extreme east of the study area, were mafic and ultramafic rocks outcrop. The other anomalies are mainly located in the Belledonne, Grandes Rousses, and Vanoise massifs. The SQI pattern doesn't provide clear evidence of a control by former mines.

4.4. Local anomalies

Figure 5 shows Pb anomalies obtained from EDA and fractals methods and SQI maps for Brandes, Peisey-Nancroix and Macôt-La Plagne Pb-Ag districts that were mined at different historical periods. Different numbers of anomalies are obtained from each method. The EDA method is the most sensitive to Pb anomalies, despite normalization to the geological background, with 22 anomalies in Brandes (Pb contents ranging from 147 $mg.kg^{-1}$ to 8900 $mg.kg^{-1}$), 5 anomalies in Peisey-Nancroix (from 139 $mg.kg^{-1}$ to 583 $mg.kg^{-1}$) and 14 anomalies in Macôt-La Plagne (from 103 $mg.kg^{-1}$ to 3200 $mg.kg^{-1}$). With the fractal approach, 9 anomalies are highlighted in Brandes, only 1 in Peisey-Nancroix and 8 in Macôt-La Plagne.

In Peisey-Nancroix, streambed sediments still have a locally high Pb content resulting in localized Pb anomalies with the EDA method, despite mine closure more than 120 years ago. However, these anomalies are not evidenced using the fractal method, and the SQIs indicate at least a fair quality of the sediments. Therefore, the spatial impact of mining activity seems very limited nowadays. In Macôt-La Plagne, higher extracted volumes and more recent mine closure are responsible for higher anomalies evidenced from the three methods: 5 samples present a poor or a marginal quality. Even though Brandes is the oldest mining district, it presents the largest Pb anomalies and the most samples with poor or marginal quality (n=9).

5. Discussion

5.1. Comparison of the statistical methods

The anomaly maps are slightly different according to the method used, as each method has its own definition of the geochemical background (Reimann and Garrett, 2005). The two single-element methods investigated provide similar results concerning the clusters with the highest anomalies, but the fractal-based model discriminates more the dataset than the EDA approach. The multi-element method (SQI) combines all single-element clusters into a single map. However, if an element is too dominant, the SQI value is driven by this element, as for arsenic in the *Série Satinée* micaschists, near Albertville (Fig. 3). Areas displaying positive anomalies with single-element approaches are not always characterized by poor SQI, thus suggesting limited dispersal of trace metals for these areas. In Peisey-Nancroix, this can be related to the rather small size of the exploitation compared to the two other sites.

At local scale, similar results are observed: (i) the fractal method is more discriminant than the EDA approach, and (ii) SQIs are generally driven by a single element (Fig. 5). In Brandes, poor and marginal sediments are clearly related to the Pb anomalies evidenced from the EDA and fractal methods. In Macôt-La Plagne, the poor and marginal samples are either related to Pb or to Ni anomalies. In Peisey-Nancroix, all sediments have a fair to good quality, despite high contents in some trace metals.

To study the spatial distribution of TMs in sediments, the choice of the statistical method must be based on the purpose of the study (Yousefi and Nykänen, 2017). Some elements better represent the rock types, such as Fe, whereas others are better

appropriated to study the occurrence of mineral deposits (e.g., Pb, Zn; Monna et al., 2014; Kirkwood et al., 2016). The EDA method is well suited to track archaeological sites and plan field prospection (Camizuli and Carranza, 2018), as it focuses on a single element and as more anomalies are evidenced. This makes it easier to highlight contamination gradients downstream a hot spot, which could be related to an ancient mining site. The fractal method can be used for screening the main clusters, as only the highest anomalies are highlighted. The concentration-area model was used for this paper, but other fractal models can be successfully used to delineate geochemical anomalies (Afzal et al., 2016; Parsa et al., 2017). The SQI introduces the probable effect on the aquatic biota and therefore can be used complementary to other environmental analyses to help determining the impact of mining activity on the ecosystem (Camizuli et al., 2014b) or more generally for river plan management (Gerber et al., 2015; Ahn et al., 2019).

5.2. Influencing parameters for geochemical anomalies at regional scale

Geochemical anomalies are either driven by natural or by anthropogenic parameters. Some specific lithologies have high background contents in one or several chemical elements, thus highlighting natural anomalies. For example, the largest As cluster is clearly related to the As-rich *Série Satinée* micaschists in this region of Albertville, and the Ni clusters are related to outcropping mafic rocks. As major tectonic contacts localize intense fluid flow, they are favorable zones for ore deposition (e.g., the contact between the Variscan crystalline basement and the Mesozoic sedimentary cover). If some of these mineralizations have been mined, many veins that were too small to be mined are contributing to local anomalies and trace metals dispersal through erosion. Mining activities enhance spreading of TMs in the environment by modifying the landscape and the hydrological network (Stöllner, 2003; Bertrand and Liébault, 2018). Downstream the largest mines and mining districts, Pb anomalies are systematics (Fig. 3). Comparison with a more precise mining database (unpublished data, R. Durand) indicates that most Pb anomalies are related to mining activity. In areas where the anomalies are disconnected with any known ore deposits or specific lithology, field prospection is required in order to determine their origin.

At regional scale, this study showed that TMs spatial distribution is either due to metal-rich lithologies, to the occurrence of mineralized veins or to former mining activity. The size and the shape of the clusters can be linked to the origin of the anomalies: mining activity and the occurrence of mineralized veins result in localized clusters, whereas metal-rich lithologies result in large clusters.

The sampling mesh size must also be taken into consideration together with the hydrographic network, the topography (Shahrestani and Mokhtari, 2017) and the climate (Montes-Avila et al., 2019) to study the spatial distribution of geochemical data. Moreover, the sediment grain size fraction is also an important parameter as metal content increases with decreasing grain size (MacKenzie and Pulford, 2002). In this study, the sampling density is ~1 sample per km², whereas in the Morvan massif, the same database shows a sampling density of 2-3 samples per km² (Lambert, 2005; Monna et al., 2014), providing a better resolution to investigate geochemical anomalies at the district scale than in the Alps. This difference in the sampling mesh is due to the larger scale and the topography of the current study area. Nonetheless, in other studies, the sampling densities are closer to 1 sample per 10 or 20 km² (Lapworth et al., 2012; Zuluaga et al., 2017), which is not dense enough to allow focusing on a district scale. Such low sampling densities help to the recognition of mineral systems during the early stages of exploration (Reimann et al., 2016).

A sampling mesh of 1 sample per km^2 is thus a minimum for detailed studies at the district scale.

5.3. 1000 years of trace metals dispersal from mining activity

Focusing on a single mining district provides information concerning the ore type, the extent of the exploitation and the extracted volume. This study focused on three Pb-Ag districts that were mined at different historical periods: the Middle Ages for Brandes, the 17th-19th c. in Peisey-Nancroix, and Modern Times in Macôt-La Plagne. At this local scale, with the EDA approach it is easier to follow the TMs path in the streambed sediments using the EDA approach. Indeed, as shown in this study, lead concentration decreases with increasing distance downstream mining areas (MacKenzie and Pulford, 2002; Camizuli et al., 2014b). As the three mining districts are situated at 1500-2000 m a.s.l. in a mountainous region, torrential streaming contributes to trace metal dispersal. The largest anomaly clusters are observed in Brandes and in Macôt-La Plagne, which were the most important mining sites during the Middle Ages and Modern Times respectively, resulting in the extraction of several hundred thousand tons of ore for each site (Meloux, 1975; pers. com. M.Ch. Bailly-Maître). Peisey-Nancroix, which was a smaller exploitation, shows much more localized number of anomalies in figure 5. Multi-element approach for this site does not allow highlighting the impacts on the aquatic ecosystem with the current dataset. Comparison of these three mining sites suggest that, at local scale, the anomalies are related to the volume of extracted ore rather than to the timing and duration of mining. This supports the idea that old mining sites still release trace metals over centuries and up to a thousand years (Camizuli et al., 2018).

As shown from SQIs, 95 % sediments analyzed in the northern French Alps have a fair to good quality, suggesting only 5% sediments could present a threat to biota. This percentage increases with more recent mining activities (Lecce and Pavlowsky, 2014). In areas showing marginal to poor sediment quality, further investigations on the bioavailable fraction are needed to evaluate this possible effect on biota (Casiot et al., 2009; Camizuli et al., 2014b; Garcia-Ordiales et al., 2014; Gutiérrez et al., 2016) and on human health (Varrica et al., 2018).

6. Concluding remarks

Three statistical methods (EDA, fractals and SQI) derived from modern mining exploration and ecological management plan were applied on geochemical data from streambed sediments of a former mining territory (the northern French Alps). These methods were used in order to highlight geochemical anomalies and to investigate the long-term dispersal of trace metals and their possible impacts on the environment up to a thousand years after mine closure. This study investigated two different scales: the regional scale (the northern French Alps) and the district scale (focusing on the three most important Pb-Ag mining sites - Brandes, Peisey-Nancroix and Macôt-La Plagne). Geochemical anomalies appear to be driven either by natural parameters, such as a metal-rich lithologies or the occurrence of hydrothermal veins related to major tectonic contacts, or by anthropogenic concentration related to former mining activity (extraction and ore processing). Some geochemical anomalies may be related to unknown ore deposits that may have a future economic potential or may have an archeological interest if complementary field surveys provide evidence of ancient mining activity.

In former mining districts, despite mine closure happened tens to a thousand years ago, local geochemical anomalies are clearly related to the remobilization of trace metals from the extraction and ore processing sites, providing evidence of very long-term remanence and dispersal of trace metals. However, the SQIs provide evidence of a very limited residual environmental impact.

Studying trace metal dispersal in ancient mining territories is thus a good tool to understand and predict long-term environmental impacts of future mining activity. Multiplying such studies in various geological and climatic contexts would contribute to improving knowledge on the parameters that control long-term trace metal dispersal. This is necessary to develop strategies to prevent them, and thus to minimize the long-term environmental impacts of mining activity.

Acknowledgements

The authors are grateful to the University of Savoie Mont-Blanc for funding a one-year post-doctoral fellowship for Estelle Camizuli and for funding the TraMines research project. This study was also funded by the French national research program EC2CO-Biohefect of the CNRS (TRACES project; grant number 183446). The authors warmly thank Robert Durand for his knowledge concerning local mines and his personal data and particularly Bruno Tourlière, in the BRGM, for providing the sediment database used for this study.

Bibliography

Afzal, P., Mirzaei, M., Yousefi, M., Adib, A., Khalajmasoumi, M., Zarifi, A.Z., Foster, P., Yasrebi, A.B., 2016. Delineation of geochemical anomalies based on stream sediment data utilizing fractal modeling and staged factor analysis. J. Afr. Earth. Sci. 119, 139-149. https://doi.org/10.1016/j.jafrearsci.2016.03.009

Agard, P., Lemoine, M., 2003. Visage des Alpes : Structure et évolution géodynamique. Commission carte géologique du monde (CCGM), Paris.

Agharezaei, M., Hezarkhani, A., 2016. Delineation of Geochemical Anomalies Based on Cu by the Boxplot as an Exploratory Data Analysis (EDA) Method and Concentration-Volume (CV) Fractal Modeling in Mesgaran Mining Area, Eastern Iran. Open J. Geol. 6, 1269. https://doi.org/10.4236/ojg.2016.610093

Ahn, J.M., Kim, S., Kim, Y.-S., 2019. Selection of priority management of rivers by assessing heavy metal pollution and ecological risk of surface sediments. Environ. Geochem. Health. https://doi.org/10.1007/s10653-019-00284-9

Antoniadis, V., Shaheen, S.M., Boersch, J., Frohne, T., Du Laing, G., Rinklebe, J., 2017. Bioavailability and risk assessment of potentially toxic elements in garden edible vegetables and soils around a highly contaminated former mining area in Germany. J. Environ. Manage. 186(2), 192-200. https://doi.org/10.1016/j.jenvman.2016.04.036

Arnaud, F., Serralongue, J., Winiarski, T., Desmet, M., Paterne, M., 2005. Pollution au plomb dans la Savoie antique (II-IIIe s. apr. J.-C.) en relation avec une installation métallurgique de la cité de Vienne. C.R. Geoscience 338, 244-252. https://doi.org/10.1016/j.crte.2005.11.008

Bailly-Maître, M.-C., 2019. L'entreprise minière de Brandes: XIe-XIVe siècles, Huez, Oisans: Extraction et transformation de minerais argentifères. Documents d'Archéologie en

527 Rhône-Alpes et en Auvergne 47, Alpara / Maison de l'Orient et de la Méditerranée,
528 Lyon.
529 Bailly-Maître, M.-C., 1989. Un coron du Moyen-Age, le site de Brandes-en-Oisans (Huez,
530 Isère). Annales de Bretagne et des pays de l'Ouest 96, 133-144.
531 https://doi.org/10.3406/abpo.1989.3319
532 Baron, S., Carignan, J., Ploquin, A., 2006. Dispersion of Heavy Metals (Metalloids) in Soils
533 from 800-Year-Old Pollution (Mont-Lozère, France). Environ. Sci. Technol. 40, 5319-
534 5326. https://doi.org/10.1021/es0606430
535 Baxter, M.J., Beardah, C.C., Westwood, S., 2000. Sample size and related issues in the
536 analysis of lead isotope data. J. Archaeolog. Sci. 27, 973-980.
537 https://doi.org/10.1006/jasc.1999.0546
538 Beane, S.J., Comber, S.D.W., Rieuwerts, J., Long, P., 2016. Abandoned metal mines and
539 their impact on receiving waters: A case study from Southwest England. Chemosphere
540 153, 294-306. https://doi.org/10.1016/j.chemosphere.2016.03.022
541 Bertrand, M., Liébault, F., 2018. Active channel width as a proxy of sediment supply from
542 mining sites in New Caledonia. Earth Surf. Processes Landforms 44(12), 67-76.
543 https://doi.org/10.1002/esp.4478
544 Besten, P.J. den, Deckere, E. de, Babut, M.P., Power, B., DelValls, T.A., Zago, C., Oen,
545 A.M.P., Heise, S., 2003. Biological effects-based sediment quality in ecological risk
546 assessment for European waters. J. Soils Sediments 3, 144-162.
547 https://doi.org/10.1065/jss2003.08.084
548 Bonham-Carter, G.F., Goodfellow, W.D., 1986. Background corrections to stream
549 geochemical data using digitized drainage and geological maps: application to selwyn
550 basin, yukon and northwest territories. J. Geochem. Explor. 25, 139-155.
551 https://doi.org/10.1016/0375-6742(86)90011-7
552 B.R.G.M. database (19 July 2019) http://sigminesfrance.brgm.fr
553 Byrne, P., Wood, P.J., Reid, I., 2012. The Impairment of River Systems by Metal Mine
554 Contamination: A Review Including Remediation Options. Crit. Rev. Environ. Sci.
555 Technol. 42, 2017-2077. https://doi.org/10.1080/10643389.2011.574103
556 Camizuli, E., Carranza, E.J.M., 2018. Exploratory Data Analysis (EDA). In: López Varela
557 S.L. and Thomas J. (Eds), The Encyclopedia of Archaeological Sciences, John Wiley
558 & Sons Inc., Hoboken. https://doi.org/10.1002/9781119188230.saseas0271
559 Camizuli, E., Monna, F., Bermond, A., Manouchehri, N., Besançon, S., Losno, R., van Oort,
560 F., Labanowski, J., Perreira, A., Chateau, C., Alibert, P., 2014a. Impact of historical
561 mining assessed in soils by kinetic extraction and lead isotopic ratios. Sci. Total
562 Environ. 472, 425-436. https://doi.org/10.1016/j.scitotenv.2013.10.103
563 Camizuli, E., Monna, F., Scheifler, R., Amiotte-Suchet, P., Losno, R., Beis, P., Bohard, B.,
564 Chateau, C., Alibert, P., 2014b. Impact of trace metals from past mining on the aquatic
565 ecosystem: A multi-proxy approach in the Morvan (France). Environ. Res. 134, 410-
566 419. https://doi.org/10.1016/j.envres.2014.07.008
567 Camizuli, E., Scheifler, R., Garnier, S., Monna, F., Losno, R., Gourault, C., Hamm, G.,
568 Lachiche, C., Delivet, G., Chateau, C., Alibert, P., 2018. Trace metals from historical
569 mining sites and past metallurgical activity remain bioavailable to wildlife today. Sci.
570 Rep. 8, 3436. https://doi.org/10.1038/s41598-018-20983-0
571 Carranza, E.J.M., 2009. Geochemical anomaly and mineral prospectivity mapping in GIS, 1st
572 ed., Handbook of exploration and environmental geochemistry 11, Elsevier,
573 Amsterdam.

574 Carranza, E.J.M., 2011. Analysis and mapping of geochemical anomalies using logratio-
575 transformed stream sediment data with censored values. J. Geochem. Explor. 110,
576 167-185. https://doi.org/10.1016/j.gexplo.2011.05.007
577 Carranza, E.J.M., Hale, M., 1997. A catchment basin approach to the analysis of
578 reconnaissance geochemical-geological data from Albay Province, Philippines. J.
579 Geochem. Explor. 60, 157-171. https://doi.org/10.1016/S0375-6742(97)00032-0
580 Casiot, C., Egal, M., Elbaz-Poulichet, F., Bruneel, O., Bancon-Montigny, C., Cordier, M.-A.,
581 Gomez, E., Aliaume, C., 2009. Hydrological and geochemical control of metals and
582 arsenic in a Mediterranean river contaminated by acid mine drainage (the Amous
583 River, France); preliminary assessment of impacts on fish (Leuciscus cephalus). Appl.
584 Geochem. 24, 787-799. https://doi.org/10.1016/j.apgeochem.2009.01.006
585 CCME, 2002. Canadian environmental quality guidelines - Summary Table (Technical
586 report). Canadian Council of Ministers of the Environment.
587 Cheng, Q., Agterberg, F.P., Ballantyne, S.B., 1994. The separation of geochemical
588 anomalies from background by fractal methods. J. Geochem. Explor. 51, 109-130.
589 https://doi.org/10.1016/0375-6742(94)90013-2
590 Ciszewski, D., Kubsik, U., Aleksander-Kwaterczak, U., 2012. Long-term dispersal of heavy
591 metals in a catchment affected by historic lead and zinc mining. J. Soils Sediments 12,
592 1445-1462. https://doi.org/10.1007/s11368-012-0558-1
593 Courtin-Nomade, A., Waltzing, T., Evrard, C., Soubrand, M., Lenain, J.-F., Ducloux, E.,
594 Ghorbel, S., Grosbois, C., Bril, H., 2016. Arsenic and lead mobility: From tailing
595 materials to the aqueous compartment. Appl. Geochem. 64, 10-21.
596 https://doi.org/10.1016/j.apgeochem.2015.11.002
597 Coward, M., Dietrich, D., Park, R.G., 1989. Alpine tectonics, Blackwell, London.
598 Darwish, M.A.G., 2017. Stream sediment geochemical patterns around an ancient gold mine
599 in the Wadi El Quleib area of the Allaqi region, south Eastern Desert of Egypt:
600 Implications for mineral exploration and environmental studies. J. Geochem. Explor.
601 175, 156-175. https://doi.org/10.1016/j.gexplo.2016.10.010
602 Debén, S., Aboal, J.R., Carballeira, A., Cesa, M., Fernández, J.A., 2017. Monitoring river
603 water quality with transplanted bryophytes: A methodological review. Ecol. Indic. 81,
604 461-470. https://doi.org/10.1016/j.ecolind.2017.06.014
605 Durand, R., 2010. Un siècle dans les mines de Savoie, Gap, Challes-les-Eaux (Savoie).
606 Durand, R., 2005. Anciennes mines et carrières souterraines de Savoie, Cléopas, Evian-les-
607 Bains.
608 Egli, M., Berger, A., Kündig, R., Krebs, R., de Castro Portes, R., Berger, R., Widmer, R.,
609 2017. The long-term interaction of mine tailings with soils and the wider environment:
610 Examples from Mont Chemin, Switzerland. J. Geochem. Explor. 182, 53-69.
611 https://doi.org/10.1016/j.gexplo.2017.08.011
612 El Azhari, A., Rhoujjati, A., EL Hachimi, M.L., 2016. Assessment of heavy metals and
613 arsenic contamination in the sediments of the Moulouya River and the Hassan II Dam
614 downstream of the abandoned mine Zeïda (High Moulouya, Morocco). J. Afr. Earth.
615 Sci. 119, 279-288. https://doi.org/10.1016/j.jafrearsci.2016.04.011
616 Elbaz-Poulichet, F., Dezileau, L., Freydier, R., Cossa, D., Sabatier, P., 2011. A 3500-Year
617 Record of Hg and Pb Contamination in a Mediterranean Sedimentary Archive (The
618 Pierre Blanche Lagoon, France). Environ. Sci. Technol. 45, 8642-8647.
619 https://doi.org/10.1021/es2004599
620 Elbaz-Poulichet, F., Resongles, E., Bancon-Montigny, C., Delpoux, S., Freydier, R., Casiot,
621 C., 2017. The environmental legacy of historic Pb-Zn-Ag-Au mining in river basins of

622 the southern edge of the Massif Central (France). Environ. Sci. Pollut. Res. 24, 20725-
623 20735. https://doi.org/10.1007/s11356-017-9669-y
624 Ettler, V., 2016. Soil contamination near non-ferrous metal smelters: A review. Appl.
625 Geochem. 64, 56-74. https://doi.org/10.1016/j.apgeochem.2015.09.020
626 Ferreira da Silva, E., Bobos, I., Xavier Matos, J., Patinha, C., Reis, A.P., Cardoso Fonseca,
627 E., 2009. Mineralogy and geochemistry of trace metals and REE in volcanic massive
628 sulfide host rocks, stream sediments, stream waters and acid mine drainage from the
629 Lousal mine area (Iberian Pyrite Belt, Portugal). Appl. Geochem. 24, 383-401.
630 https://doi.org/10.1016/j.apgeochem.2008.12.001
631 Garcia-Ordiales, E., Loredo, J., Esbrí, J.M., Lominchar, M.A., Millan, R., Higueras, P., 2014.
632 Stream bottom sediments as a means to assess metal contamination in the historic
633 mining district of Almadén (Spain). Int. J. Min. Reclam. Environ. 28, 357-376.
634 https://doi.org/10.1080/17480930.2014.967917
635 Garrett, R.G., 2016. rgr: Applied Geochemistry EDA.
636 Garrett, R.G., 2013. The 'rgr' package for the R Open Source statistical computing and
637 graphics environment - a tool to support geochemical data interpretation. Geochem.
638 Explor. Environ. Anal. 13, 355-378. https://doi.org/10.1144/geochem2011-106
639 Gasquet, D., Rossi, M., 2015. Environmental Impacts and Management of Ancient
640 Abandoned Mines in the French Alps. Proceeding of the 13th SGA Biennal Meeting,
641 24-27 August 2015 Nancy, France, 1523-1526.
642 Gbolo, P., Lopez, D.L., 2015. Analysis of trace elements pollution within streambed
643 sediments from the Shade River Watershed, southeastern Ohio. Environ. Earth Sci.
644 73, 7193-7204. https://doi.org/10.1007/s12665-014-3899-9
645 Gerber, R., Smit, N.J., van Vuren, J.H.J., Nakayama, S.M.M., Yohannes, Y.B., Ikenaka, Y.,
646 Ishizuka, M., Wepener, V., 2015. Application of a Sediment Quality Index for the
647 assessment and monitoring of metals and organochlorines in a premier conservation
648 area. Environ. Sci. Pollut. Res. 22, 19971-19989. https://doi.org/10.1007/s11356-015-
649 5206-z
650 Giguet-Covex, C., Arnaud, F., Poulenard, J., Disnar, J.-R., Delhon, C., Francus, P., David,
651 F., Enters, D., Rey, P.-J., Delannoy, J.-J., 2011. Changes in erosion patterns during
652 the Holocene in a currently treeless subalpine catchment inferred from lake sediment
653 geochemistry (Lake Anterne, 2063 m a.s.l., NW French Alps): The role of climate and
654 human activities. Holocene 21, 651-665. https://doi.org/10.1177/0959683610391320
655 Gimard, A., 1987. Les travaux romains des mines de plomb argentifère de Macôt-la-Plagne.
656 Proceedings of the meeting Mines et métallurgie en Gaule et dans les Provinces
657 Romaines, 26-27 April 1986 Paris, France, 98-113.
658 Gonçalves, M.A., Mateus, A., Pinto, F., Vieira, R., 2017. Using multifractal modelling,
659 singularity mapping, and geochemical indexes for targeting buried mineralization:
660 Application to the W-Sn Panasqueira ore-system, Portugal. J. Geochem. Explor. 189,
661 42-53. https://doi.org/10.1016/j.gexplo.2017.07.008
662 Gutiérrez, M., Mickus, K., Camacho, L.M., 2016. Abandoned Pb-Zn mining wastes and their
663 mobility as proxy to toxicity: A review. Sci. Total Environ. 565, 392-400.
664 https://doi.org/10.1016/j.scitotenv.2016.04.143
665 Helsel, D.R., 2012. Statistics for censored environmental data using Minitab and R, Wiley
666 series in statistics in practice. John Wiley & Sons, Hoboken.
667 Hoang, A.H., Nguyen, T.T., 2016. Identification of Spatial Distribution of Geochemical
668 Anomalies Based on GIS and C-A Fractal Model - A Case Study of Jiurui Copper
669 Mining Area. J. Geosci. Geomatics 4, 36-41. https://doi.org/10.12691/jgg-4-2-3

Horak, J., Hejcman, M., 2016. Contamination Characteristics of the Confluence of Polluted and Unpolluted Rivers-Range and Spatial Distribution of Contaminants of a Significant Mining Centre (Kutná Hora, Czech Republic). Soil Water Res. 11, 243. https://doi.org/10.17221/118/2015-SWR

Hudson-Edwards, K.A., 2003. Sources, mineralogy, chemistry and fate of heavy metal-bearing particles in mining-affected river systems. Mineral. Mag. 67, 205-217. https://doi.org/10.1180/0026461036720095

Kabata-Pendias, A., 2011. Trace elements in soils and plants, 4th ed. CRC Press, Taylor & Francis Group, Boca Raton

Kirkwood, C., Everett, P., Ferreira, A., Lister, B., 2016. Stream sediment geochemistry as a tool for enhancing geological understanding: An overview of new data from south west England. J. Geochem. Explor. 163, 28-40. https://doi.org/10.1016/j.gexplo.2016.01.010

Kossoff, D., Hudson-Edwards, K.A., Howard, A.J., Knight, D., 2016. Industrial mining heritage and the legacy of environmental pollution in the Derbyshire Derwent catchment: Quantifying contamination at a regional scale and developing integrated strategies for management of the wider historic environment. J. Archaeolog. Sci.: Rep. 6, 190-199. https://doi.org/10.1016/j.jasrep.2016.02.007

Lambert, A., 2005. Les données géochimiques et alluvionnaires de l'Inventaire minier du territoire national. Constitution d'une base de données exhaustive. Final report No. RP-53546-FR, BRGM, Orléans.

Lapworth, D.J., Knights, K.V., Key, R.M., Johnson, C.C., Ayoade, E., Adekanmi, M.A., Arisekola, T.M., Okunlola, O.A., Backman, B., Eklund, M., Everett, P.A., Lister, R.T., Ridgway, J., Watts, M.J., Kemp, S.J., Pitfield, P.E.J., 2012. Geochemical mapping using stream sediments in west-central Nigeria: Implications for environmental studies and mineral exploration in West Africa. Appl. Geochem. 27, 1035-1052. https://doi.org/10.1016/j.apgeochem.2012.02.023

Lecce, S.A., Pavlowsky, R.T., 2014. Floodplain storage of sediment contaminated by mercury and copper from historic gold mining at Gold Hill, North Carolina, USA. Geomorphology 206, 122-132. https://doi.org/10.1016/j.geomorph.2013.10.004

MacDonald, D.D., Ingersoll, C.G., Berger, T.A., 2000. Development and Evaluation of Consensus-Based Sediment Quality Guidelines for Freshwater Ecosystems. Arch. Environ. Contam. Toxicol. 39, 20-31. https://doi.org/10.1007/s002440010075

MacKenzie, A.B., Pulford, I.D., 2002. Investigation of contaminant metal dispersal from a disused mine site at Tyndrum, Scotland, using concentration gradients and stable Pb isotope ratios. Appl. Geochem. 17, 1093-1103. https://doi.org/10.1016/S0883-2927(02)00007-0

Madejón, P., Domínguez, M.T., Madejón, E., Cabrera, F., Marañón, T., Murillo, J.M., 2018. Soil-plant relationships and contamination by trace elements: A review of twenty years of experimentation and monitoring after the Aznalcóllar (SW Spain) mine accident. Sci. Total Environ. 625, 50-63. https://doi.org/10.1016/j.scitotenv.2017.12.277

Mariet, A.-L., Bégeot, C., Gimbert, F., Gauthier, J., Fluck, P., Walter-Simonnet, A.-V., 2016. Past mining activities in the Vosges Mountains (eastern France): Impact on vegetation and metal contamination over the past millennium. Holocene 26, 1225-1236. https://doi.org/10.1177/0959683616638419

Mariet, A.-L., Pauget, B., de Vaufleury, A., Bégeot, C., Walter-Simonnet, A.-V., Gimbert, F., 2017. Using bioindicators to assess the environmental risk of past mining activities in the Vosges Mountains (France). Ecol. Indic. 75, 17-26. https://doi.org/10.1016/j.ecolind.2016.11.042

718 Marthaler, M., 2005. The Alps and our Planet : The African Matterhorn, a geological story,
719 Lep, Lausanne.
720 Marvin, C., Grapentine, L., Painter, S., 2004. Application of a Sediment Quality Index to the
721 Lower Laurentian Great Lakes. Environ. Monit. Assess. 91, 1-16.
722 https://doi.org/10.1023/B:EMAS.0000009227.39355.aa
723 McConnell, J.R., Wilson, A.I., Stohl, A., Arienzo, M.M., Chellman, N.J., Eckhardt, S.,
724 Thompson, E.M., Pollard, A.M., Steffensen, J.P., 2018. Lead pollution recorded in
725 Greenland ice indicates European emissions tracked plagues, wars, and imperial
726 expansion during antiquity. PNAS 115, 5726-5731.
727 https://doi.org/10.1073/pnas.1721818115
728 Meloux, J., 1975. Alpes-Nord. Bilan synthétique de dix années de prospection, Report No.
729 75- RME- 023- FE, BRGM, Orléans.
730 Monna, F., Camizuli, E., Nedjai, R., Cattin, F., Petit, C., Guillaumet, J.-P., Jouffroy-Bapicot,
731 I., Bohard, B., Chateau, C., Alibert, P., 2014. Tracking archaeological and historical
732 mines using mineral prospectivity mapping. J. Archaeolog. Sci. 49, 57-69.
733 https://doi.org/10.1016/j.jas.2014.04.022
734 Montes-Avila, I., Espinosa-Serrano, E., Castro-Larragoitia, J., Lázaro, I., Cardona, A., 2019.
735 Chemical mobility of inorganic elements in stream sediments of a semiarid zone
736 impacted by ancient mine residues. Appl. Geochem. 100, 8-21.
737 https://doi.org/10.1016/j.apgeochem.2018.11.002
738 Mortazavi, S., Saberinasab, F., 2017. Heavy metals assessment of surface sediments in
739 Mighan wetland using the Sediment Quality Index. Ecopersia 5(2), 1761-1770.
740 https://doi.org/10.18869/modares.Ecopersia.5.2.1761
741 Moulin, B., Thirault, É., Vital, J., 2012. Quatre années de prospection sur les extractions de
742 cuivre de l'âge du Bronze ancien dans le massif des Rousses en Oisans (Isère et
743 Savoie, France). Proceedings of the 9th Rencontres Méridionales de Préhistoire
744 Récente, 8-9 October 2010, Saint-Georges-de-Didonne, France, 341-369.
745 Nicolas, J., 1978. La Savoie au XVIIIe siècle, tome 2, Inflexions au siècle des Lumières,
746 Maloine, Paris.
747 Parsa, M., Maghsoudi, A., Yousefi, M., Carranza, E.J.M., 2017. Multifractal interpolation and
748 spectrum-area fractal modeling of stream sediment geochemical data: Implications for
749 mapping exploration targets. J. Afr. Earth. Sci. 128, 5-15.
750 https://doi.org/10.1016/j.jafrearsci.2016.11.021
751 Potra, A., Dodd, J.W., Ruhl, L.S., 2017. Distribution of trace elements and Pb isotopes in
752 stream sediments of the Tri-State mining district (Oklahoma, Kansas, and Missouri),
753 USA. Appl. Geochem. 82, 25-37. https://doi.org/10.1016/j.apgeochem.2017.05.005
754 Py, V., Véron, A., Edouard, J.-L., Beaulieu, J.-L. de, Ancel, B., Segard, M., Durand, A.,
755 Leveau, P., 2014. Interdisciplinary characterisation and environmental imprints of
756 mining and forestry in the upper Durance valley (France) during the Holocene. Quat.
757 Int. 353, 74-97. https://doi.org/10.1016/j.quaint.2014.05.002
758 QGIS Development Team, 2017. QGIS Geographic Information System. Open Source
759 Geospatial Foundation.
760 R Core Team, 2017. R: A Language and Environment for Statistical Computing. R
761 Foundation for Statistical Computing, Vienna, Austria.
762 Reimann, C., Filzmoser, P., Garrett, R.G., Dutter, R., 2008. Statistical data analysis
763 explained: applied environmental statistics with R, John Wiley & Sons, Ltd, Chichester.
764 Reimann, C., Garrett, R.G., 2005. Geochemical background—concept and reality. Sci. Total
765 Environ. 350, 12-27. https://doi.org/10.1016/j.scitotenv.2005.01.047

766 Reimann, C., Ladenberger, A., Birke, M., Caritat, P. de, 2016. Low density geochemical
767 mapping and mineral exploration: application of the mineral system concept.
768 Geochem. Explor. Environ. Anal. 16, 48-61. https://doi.org/10.1144/geochem2014-327
769 Resongles, E., Casiot, C., Freydier, R., Dezileau, L., Viers, J., Elbaz-Poulichet, F., 2014.
770 Persisting impact of historical mining activity to metal (Pb, Zn, Cd, Tl, Hg) and
771 metalloid (As, Sb) enrichment in sediments of the Gardon River, Southern France. Sci.
772 Total Environ. 481, 509-521. https://doi.org/10.1016/j.scitotenv.2014.02.078
773 Rosman, K.J.R., Chisholm, W., Hong, S., Candelone, J.-P., Boutron, C.F., 1997. Lead from
774 Carthaginian and Roman Spanish Mines Isotopically Identified in Greenland Ice Dated
775 from 600 B.C. to 300 A.D.†. Environ. Sci. Technol. 31, 3413-3416.
776 https://doi.org/10.1021/es970038k
777 Rossi, M., Gasquet, D., 2014. Panorama géologique des exploitations minières dans les
778 Alpes françaises. Collection EDYTEM 17, 23-40.
779 https://doi.org/10.3406/edyte.2014.1271
780 Schibler, J., Breitenlechner, E., Deschler-Erb, S., Goldenberg, G., Hanke, K., Hiebel, G.,
781 Hüster Plogmann, H., Nicolussi, K., Marti-Grädel, E., Pichler, S., Schmidl, A., Schwarz,
782 S., Stopp, B., Oeggl, K., 2011. Miners and mining in the Late Bronze Age: a
783 multidisciplinary study from Austria. Antiquity 85, 1259-1278.
784 https://doi.org/10.1017/S0003598X00062049
785 Schreck, E., Viers, J., Blondet, I., Auda, Y., Macouin, M., Zouiten, C., Freydier, R.,
786 Dufréchou, G., Chmeleff, J., Darrozes, J., 2020. Tillandsia usneoides as biomonitors of
787 trace elements contents in the atmosphere of the mining district of Cartagena-La
788 Unión (Spain): New insights for element transfer and pollution source tracing.
789 Chemosphere 241, 124955. https://doi.org/10.1016/j.chemosphere.2019.124955
790 Shahrestani, S., Mokhtari, A.R., 2017. Dilution correction equation revisited: The impact of
791 stream slope, relief ratio and area size of basin on geochemical anomalies. J. Afr.
792 Earth. Sci. 128, 16-26. https://doi.org/10.1016/j.jafrearsci.2016.06.019
793 Stöllner, T., 2003. Mining and economy: a discussion of spatial organisations and structures
794 of early raw material exploitation. Der Anschnitt 16, 415-446.
795 Tukey, J.W., 1977. Exploratory data analysis, Addison-Wesley series in behavioral science:
796 quantitative methods. Addison-Wesley Publishing Company, Reading.
797 Varrica, D., Dongarrà, G., Alaimo, M.G., Monna, F., Losno, R., Sanna, E., De Giudici, G.,
798 Tamburo, E., 2018. Lead isotopic fingerprint in human scalp hair: The case study of
799 Iglesias mining district (Sardinia, Italy). Sci. Total Environ. 613-614, 456-461.
800 https://doi.org/10.1016/j.scitotenv.2017.09.106
801 West, S., Charman, D.J., Grattan, J.P., Cherburkin, A.K., 1997. Heavy Metals in Holocene
802 Peats from South West England: Detecting Mining Impacts and Atmospheric Pollution.
803 Water Air Soil Pollut. 100, 343-353. https://doi.org/10.1023/A:1018393013619
804 Yousefi, M., Nykänen, V., 2017. Introduction to the special issue: GIS-based mineral
805 potential targeting. J. Afr. Earth. Sci. 128, 1-4.
806 https://doi.org/10.1016/j.jafrearsci.2017.02.023
807 Yusta, I., Velasco, F., Herrero, J.-M., 1998. Anomaly threshold estimation and data
808 normalization using EDA statistics: application to lithogeochemical exploration in
809 Lower Cretaceous Zn-Pb carbonate-hosted deposits, Northern Spain. Appl. Geochem.
810 13, 421-439. https://doi.org/10.1016/S0883-2927(97)00095-4
811 Zuluaga, M.C., Norini, G., Lima, A., Albanese, S., David, C.P., De Vivo, B., 2017. Stream
812 sediment geochemical mapping of the Mount Pinatubo-Dizon Mine area, the

Philippines: Implications for mineral exploration and environmental risk. J. Geochem. Explor. 175, 18-35. https://doi.org/10.1016/j.gexplo.2016.12.012

Zuo, R., Wang, J., 2016. Fractal/multifractal modeling of geochemical data: A review. J. Geochem. Explor. 164, 33-41. https://doi.org/10.1016/j.gexplo.2015.04.010

Figure captions

Figure 1. Overview of the study area, showing the location of the three targeted sites (Br for Brandes, MP for Macôt-La Plagne, PN for Peisey-Nancroix) and other mines cited in the text (Ch for Chalanches, Ro for Rocheray, SGH for St-Georges d'Hurtières). (a) Simplified lithological map of the northern French Alps modified from the 1:1 000 000 BRGM geological map and OneGeology data, (b) mining sites and ore deposits from the BRGM database (topography from BD ALTI® 25 m; hydrographic network from BD Carthage®), and (c) BRGM sampling location of streambed sediments. The contoured area in (a) and (b) delimits the BRGM streambed sediment database.

Figure 2. Example of data standardization according to the lithological units for Pb. (a) Data without standardization, (b) data after standardization, UIF: upper inner fence, UOF: upper outer fence. Sup. deposits stands for superficial deposits.

Figure 3. Anomaly maps for As, Cu, and Pb resulting from EDA (a) and fractal (b) approaches. Only the highest anomaly categories were reported to facilitate reading. See legend of the lithological map in Fig. 1.

Figure 4. Sediment Quality Index maps highlighting the poor and marginal anomalies, and showing location of the mines. See legend of the lithological map in Fig. 1.

Figure 5. Comparison of Pb anomaly distributions from the EDA and fractal methods, and SQI maps for the three studied mining districts: (a) the medieval site of Brandes, (b) the historical Peisey-Nancroix mine, and (c) the modern Macôt-La Plagne mine.

Supplementary data

Figure S1. Anomaly maps for Ni and Zn resulting from EDA (a) and fractal (b) approaches. Only the high anomaly categories were reported to facilitate reading. See legend of the lithological map in Fig. 1.

Tables and table captions

Table 1.

	Fe2O3	MnO	As	Cd	Cr	Cu	Ni	Pb	Zn
	%	%	mg.kg^{-1}	mg.kg^{-1}	mg.kg^{-1}	mg.kg^{-1}	mg.kg^{-1}	mg.kg^{-1}	mg.kg^{-1}
Limit of detection	0.1	0.01	20	2	10	10	10	10	10
Min.	<0.1	<0.01	<20	<2	<10	<10	<10	<10	<10
Q1	4.4	0.09	29	<2	45	22	28	32	86
Median (Q2)	5.7	0.13	42	<2	60	32	40	43	112
Mean	5.8	0.16	59	<2	71	39	49	66	138
Q3	7	0.18	62	<2	80	45	55	60	149
Max.	25	2.7	1076	45	1700	1530	1571	8900	8190
Skewness	0.71 (-1.87)	5.07 (-0.11)	5.66 (0.72)	nc	8.98 (0.07)	14.33 (0.05)	11.92 (0.07)	23.93 (1.58)	23.99 (-0.64)
nb. cen (\%)	3 (0.04)	21 (0.3)	942 (13.7)	6411 (93)	56 (0.8)	397 (5.8)	215 (3)	45 (0.7)	93 (1.3)
European topsoils (mean)[1]			11.6	0.28	94.8	17.3	37	32	68.1
TEC [2]			9.79	0.99	43.4	31.6	22.7	35.8	121
PEC [3]			33	4.98	111	149	48.6	128	459

[1] Kabata-Pendias (2011)

[2] MacDonald et al. (2000)

[3] MacDonald et al. (2000)

Table 1. Descriptive statistics for Fe2O3, MnO, As, Cd, Cr, Cu, Ni, Pb and Zn concentrations on the BRGM Alps dataset. Skewness after log10-transformation is indicated between parentheses, nb. cen are the number of data below the limit of detection and between parenthesis their corresponding percentages. nc stands for not calculated, TEC for Threshold Effect Concentration and PEC for Probable Effect Concentration. Data from http://sigminesfrance.brgm.fr. Concentrations found in the literature are also indicated (Kabata-Pendias, 2011; MacDonald et al., 2000).

874
875

Table 2.

Categories	zAs			zCu			zNi			zPb			zZn		
	Cut level	*n*	%	Cut level	*n*	%	Cut level	*n*	%	Cut level	*n*	%	Cut level	*n*	%
Far low outliers	< 0.51	0	0.0	< 0.48	0	0	< 0.64	0	0	< 0.75	0	0	< 0.93	0	0
Near low outliers	0.51 - 1.06	29	0.4	0.48 - 1	2	0.03	0.64 - 1.25	59	0.9	0.75 - 1.41	50	0.7	0.93 - 1.66	170	2.5
Low background	1.06 - 2.21	1711	24.8	1 - 2.11	1764	25.6	1.25 - 2.43	1724	25.0	1.41 - 2.65	1674	24.3	1.66 - 2.98	1570	22.8
Background (Q1-Q3)	2.21 - 3.6	**3439**	49.9	2.11 - 3.46	**3448**	50.0	2.43 - 3.79	**3394**	49.2	2.65 - 4.03	**3459**	50.2	2.98 - 4.39	**3442**	49.9
High background	3.6 - 7.49	1354	19.6	3.46 - 7.26	1516	22.0	3.79 - 7.39	1507	21.9	4.03 - 7.56	1361	19.7	4.39 - 7.84	1407	20.4
Near high outliers	7.49 - 15.59	298	4.3	7.26 - 15.25	139	2.0	7.39 - 14.41	164	2.4	7.56 - 14.17	231	3.4	7.84 - 14.03	236	3.4
Far high outliers	> 15.59	61	0.9	> 15.25	23	0.3	> 14.41	44	0.6	> 14.17	117	1.7	> 14.03	67	1.0

876
877 **Table 2.** Cut levels obtained from the computation of the log-transformed standardized data
878 (EDA approach). The number of samples in each category is specified. The seven
879 categories are based on the Tukey boxplot (Camizuli and Carranza, 2018; Tukey, 1977).
880
881

Table 3.

						nb. of samples		
As	range	slope	intercept	r-squared	interpretation	Akima	BRGM dataset	%
1	$<$ 25	-1.163	116.79	0.998	Very low background	602	1400	20.3 %
2	25-32	-1.733	131.62	0.998	Low background	590	776	28.0 %
3	32-41	-2.327	150.53	1	Low background	1022	1151	
4	41-60	-1.61	119.58	0.993	Background	1494	1738	37.6 %
5	60-82	-0.824	73.43	0.985	Background	839	852	
6	82-103	-0.136	19.23	0.995	High background	132	309	12.1 %
7	103-122	-0.063	11.79	0.961	High background	57	151	
8	122-213	-0.033	7.81	0.925	High background	138	284	
9	213-273	-0.009	3.28	0.879	High background	31	88	
10	273-463	-0.004	1.76	0.859	High anomaly	34	108	1.6 %
11	$>$ 463	-0.002	1.07	0.968	Very high anomaly	5	35	0.5 %

						nb. of samples		
Cu	range	slope	intercept	r-squared	interpretation	Akima	BRGM dataset	%
1	$<$ 13	-0.774	105.71	0.996	Very low background	212	661	9.6 %
2	13-19	-1.227	111.83	0.998	Low background	371	684	39.4 %
3	19-24	-2.328	132.44	0.999	Low background	590	791	
4	24-31	-3.109	151.41	0.999	Low background	1062	1240	
5	31-43	-2.799	138.99	0.978	Background	1616	1635	46.6 %
6	43-66	-0.765	52.84	0.941	Background	820	1230	
7	66-90	-0.165	15.94	0.955	Background	194	348	
8	90-126	-0.044	5.35	0.902	High background	65	197	2.9 %
9	$>$ 126	-0.001	0.33	0.649	High anomaly	14	106	1.5 %

						nb. of samples		
Ni	range	slope	intercept	r-squared	interpretation	Akima	BRGM dataset	%
1	$<$ 15	-0.615	104.91	0.986	Very low background	227	540	7.8 %
2	15-24	-1.337	115.68	0.995	Low background	604	801	28.4 %
3	24-33	-2.027	132.05	0.999	Low background	890	1156	
4	33-45	-2.235	138.18	0.999	Background	1326	1672	51.8 %
5	45-72	-1.083	84.08	0.958	Background	1363	1901	
6	72-125	-0.146	20.32	0.946	High background	372	613	11.4 %
7	125-256	-0.016	4.97	0.947	High background	100	165	
8	256-325	-0.003	2.12	0.955	High background	13	11	
9	325-372	-0.004	2.17	0.957	High anomaly	8	0	0.4 %
10	372-694	-0.002	1.41	0.93	High anomaly	28	26	
11	$>$ 694	-3.99E-04	0.5	0.854	Very high anomaly	13	7	0.1 %

						nb. of samples		
Pb	range	slope	intercept	r-squared	interpretation	Akima	BRGM dataset	%
1	$<$ 20	-0.21	102.46	0.826	Very low background	107	356	5.2 %
2	20-28	-1.161	122.02	0.974	Low background	458	852	32.3 %
3	28-37	-2.58	161.26	0.999	Low background	1147	1372	
4	37-55	-2.153	142.9	0.989	Background	1876	2272	48.7 %
5	55-77	-0.944	77.79	0.969	Background	925	1085	
6	77-162	-0.092	14.39	0.888	High background	363	719	12.8 %
7	162-369	-0.006	2.11	0.914	High background	56	160	
8	369-890	-2.98E-04	0.35	0.955	High anomaly	7	42	0.6 %
9	$>$ 890	-8.94E-05	0.17	0.822	Very high anomaly	5	34	0.5 %

						nb. of samples		
Zn	range	slope	intercept	r-squared	interpretation	Akima	BRGM dataset	%
1	$<$ 21	-0.043	100.2	0.947	Very low background	33	132	3.9 %
2	21-43	-0.059	100.76	0.89	Very low background	67	137	
3	43-64	-0.257	110.21	0.928	Low background	238	422	22.2 %
4	64-87	-0.755	142.67	0.988	Low background	855	1108	
5	87-111	-1.204	181.67	0.998	Background	1383	1584	64.6 %
6	111-218	-0.463	91.6	0.882	Background	2130	2867	

7	218-294	-0.032	11.56	0.966	High background	125	293	7.4 %
8	294-465	-0.011	5.25	0.893	High background	89	217	
9	465-597	-0.003	1.61	0.968	High anomaly	18	53	0.8 %
10	$>$ 597	-1.81E-04	0.22	0.975	Very high anomaly	6	79	1.1 %

Table 3. Summary of the parameters for the concentration-area plot of each study element (fractal approach).

888
889

Table 4.

Category	Range	Percentage	Nb of samples
Poor	]-1,45]	1.38	95
Marginal	]45,60]	3.93	271
Fair	]60,80]	31.36	2161
Good	]80,95]	39.61	2730
Excellent	]95,100]	23.72	1635

890
891 **Table 4.** Percentage and number of samples in each SQI category
892

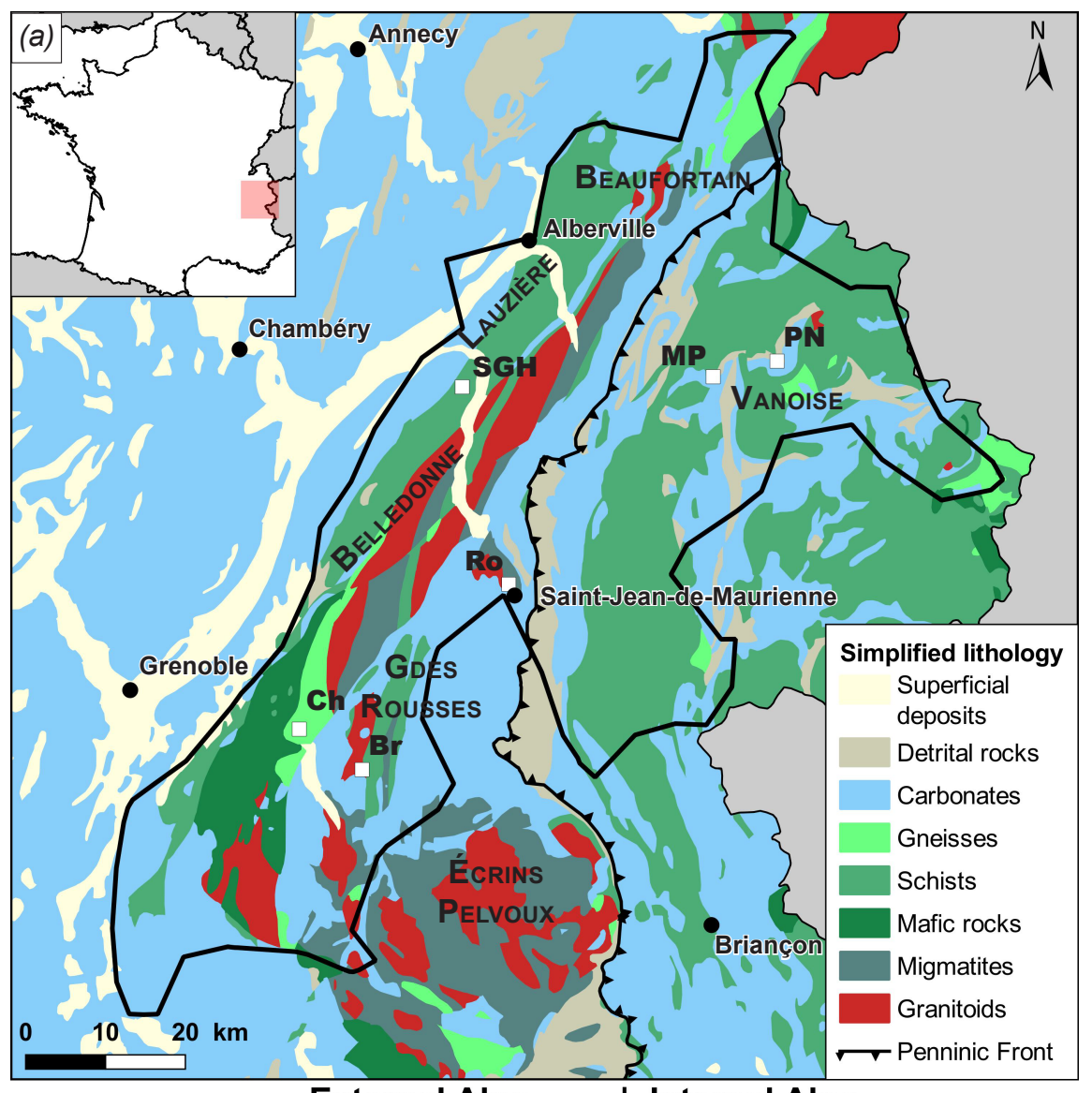
(a)
N
Annecy
Beaufortain
Alberville
Lauzière
Chambéry
SGH
MP
PN
Vanoise
Belledonne
Ro
Saint-Jean-de-Maurienne
Grenoble
Gdes Rousses
Ch
Br
Écrins
Pelvoux
Briançon
0 10 20 km
Simplified lithology
Superficial deposits
Detrital rocks
Carbonates
Gneisses
Schists
Mafic rocks
Migmatites
Granitoids
Penninic Front
External Alps | Internal Alps

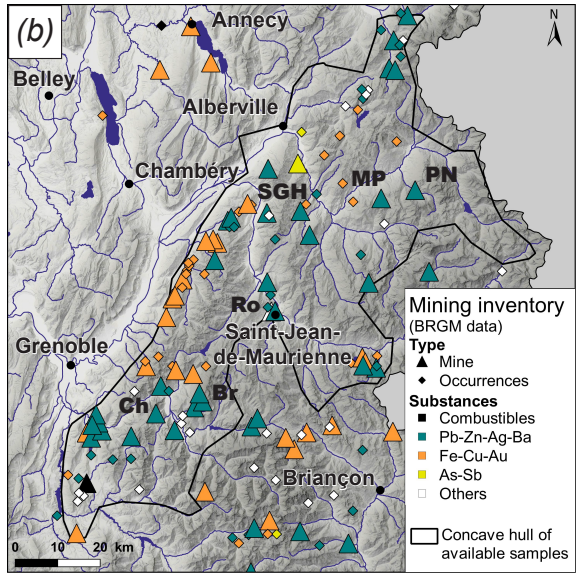
(b)
N
Annecy
Belley
Alberville
Chambéry
SGH
MP
PN
Ro
Saint-Jean-de-Maurienne
Grenoble
Ch
Br
Briançon
Mining inventory
(BRGM data)
Type
Mine
Occurrences
Substances
Combustibles
Pb-Zn-Ag-Ba
Fe-Cu-Au
As-Sb
Others
Concave hull of available samples
0 10 20 km

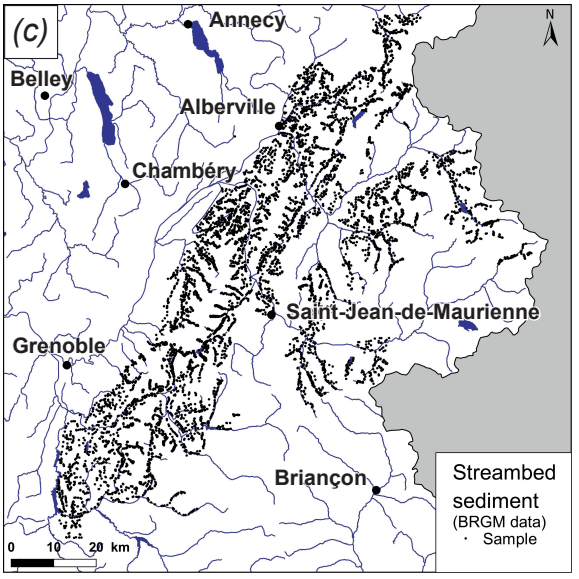
(c)
N
Annecy
Belley
Alberville
Chambéry
Saint-Jean-de-Maurienne
Grenoble
Briançon
Streambed sediment
(BRGM data)
Sample
0 10 20 km

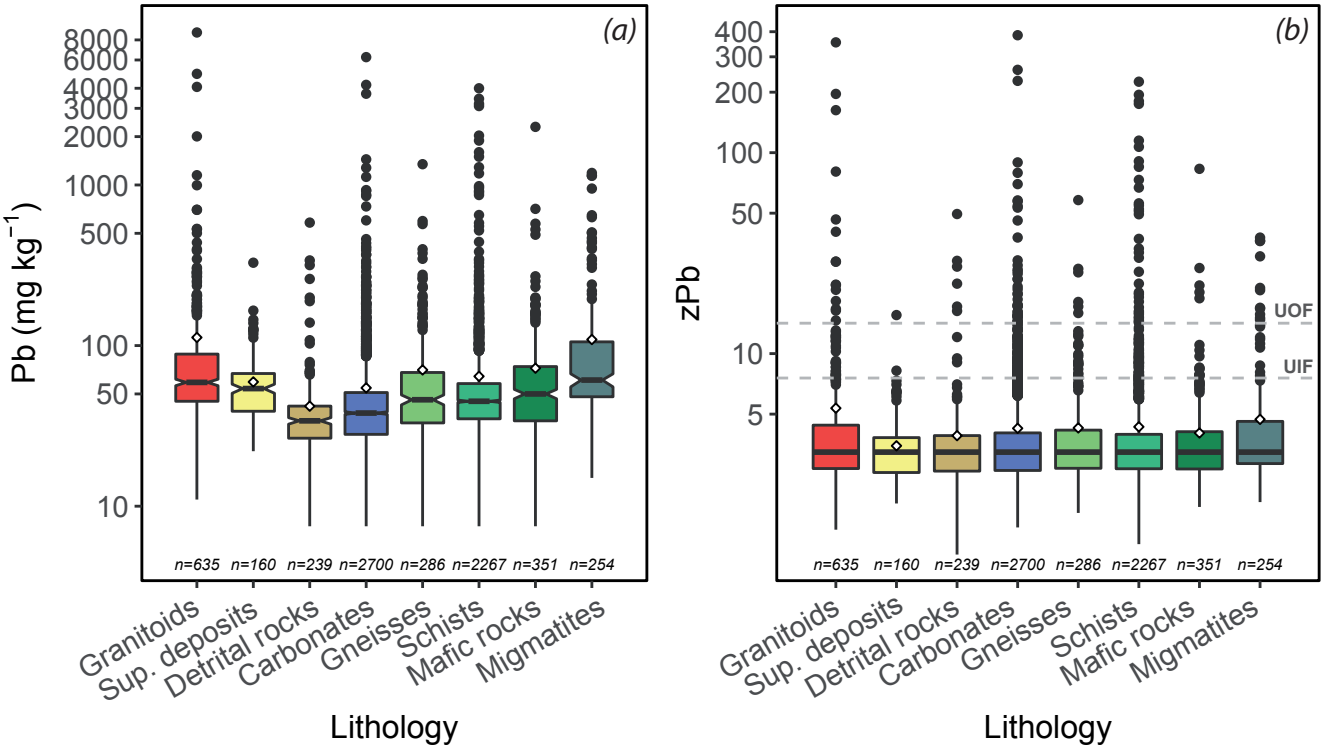
(a)
Pb (mg kg^{-1})
8000
6000
4000
3000
2000
1000
500
100
50
10
n=635 n=160 n=239 n=2700 n=286 n=2267 n=351 n=254
Granitoids
Sup. deposits
Detrital rocks
Carbonates
Gneisses
Schists
Mafic rocks
Migmatites
Lithology
(b)
zPb
400
300
200
100
50
10
5
UOF
UIF
n=635 n=160 n=239 n=2700 n=286 n=2267 n=351 n=254
Granitoids
Sup. deposits
Detrital rocks
Carbonates
Gneisses
Schists
Mafic rocks
Migmatites
Lithology

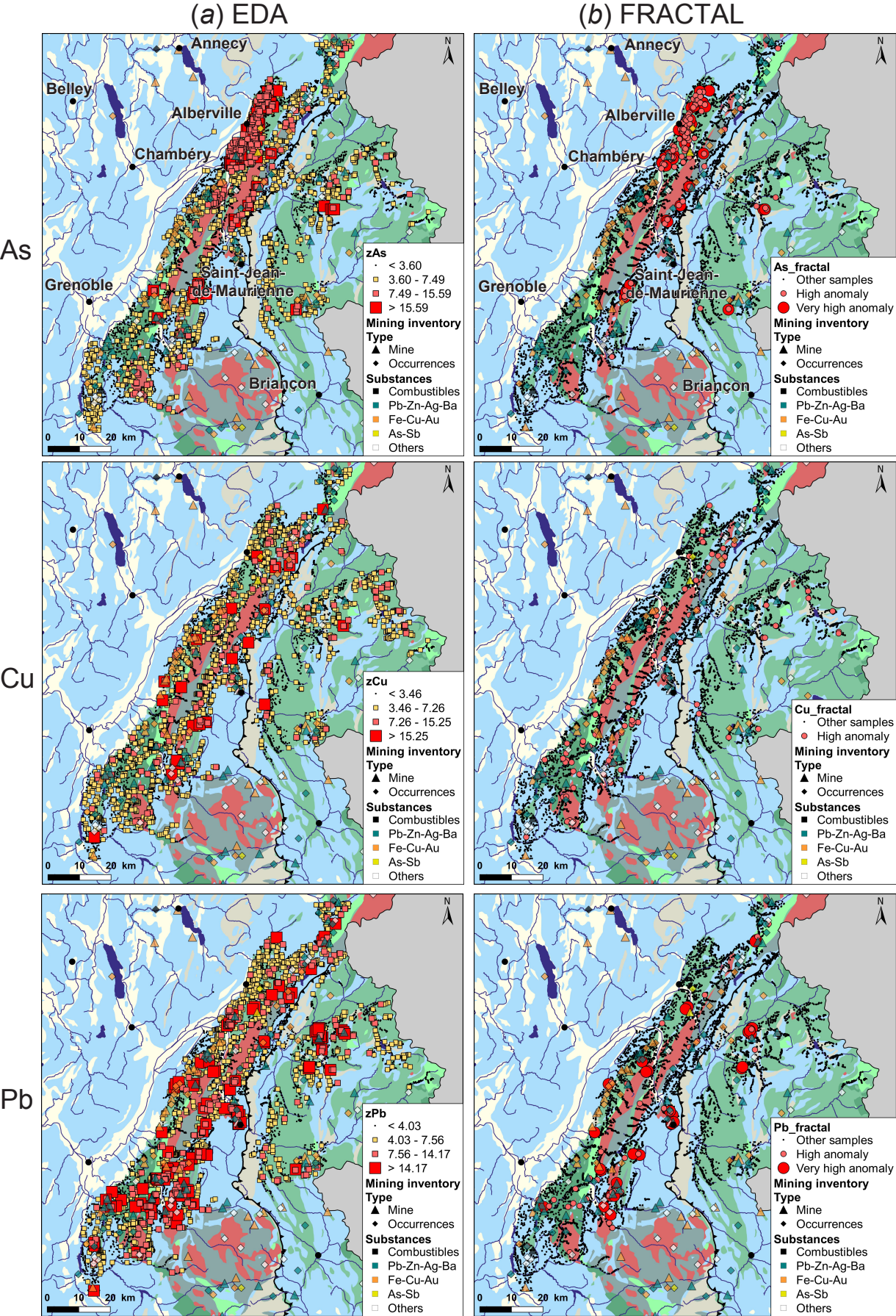
(a) EDA
(b) FRACTAL
As
Cu
Pb
Annecy
Belley
Alberville
Chambéry
Grenoble
Saint-Jean-de-Maurienne
Briançon
N
0 10 20 km
zAs
< 3.60
3.60 - 7.49
7.49 - 15.59
> 15.59
As_fractal
Other samples
High anomaly
Very high anomaly
zCu
< 3.46
3.46 - 7.26
7.26 - 15.25
> 15.25
Cu_fractal
Other samples
High anomaly
zPb
< 4.03
4.03 - 7.56
7.56 - 14.17
> 14.17
Pb_fractal
Other samples
High anomaly
Very high anomaly
Mining inventory
Type
Mine
Occurrences
Substances
Combustibles
Pb-Zn-Ag-Ba
Fe-Cu-Au
As-Sb
Others

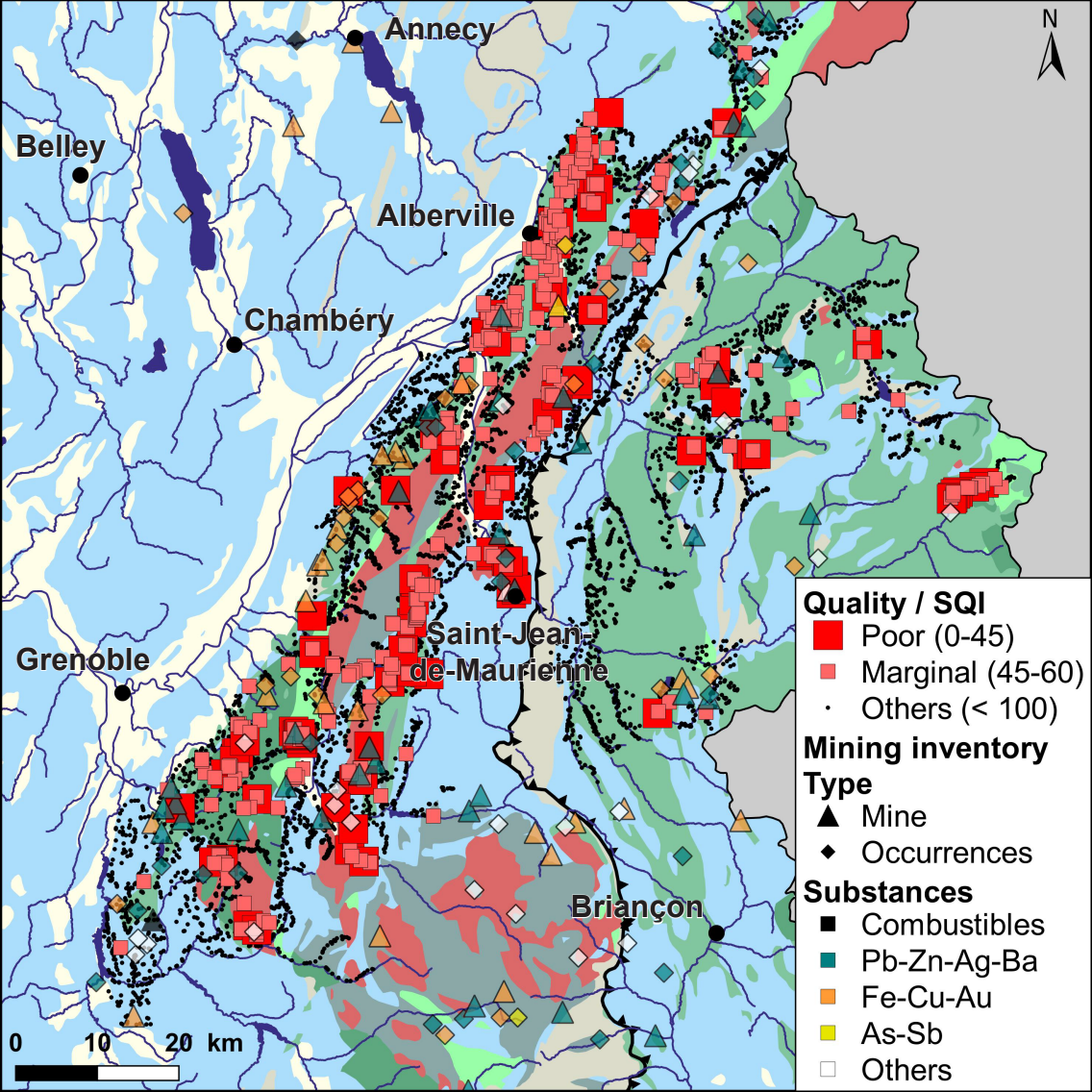
Annecy
Belley
Alberville
Chambéry
Grenoble
Saint-Jean-de-Maurienne
Briançon
N
0 10 20 km
Quality / SQI
Poor (0-45)
Marginal (45-60)
Others (< 100)
Mining inventory
Type
Mine
Occurrences
Substances
Combustibles
Pb-Zn-Ag-Ba
Fe-Cu-Au
As-Sb
Others

(*a*) **Brandes**
11th-17th
> 900 000 t. of dumps

(*b*) **Peisey-Nancroix**
1644-1865
22 000 t. Pb + 53 t. Ag

(*c*) **Macôt-La Plagne**
1810-1973
126 600 t. Pb + 350 t. Ag

EDA

Fractal

SQI

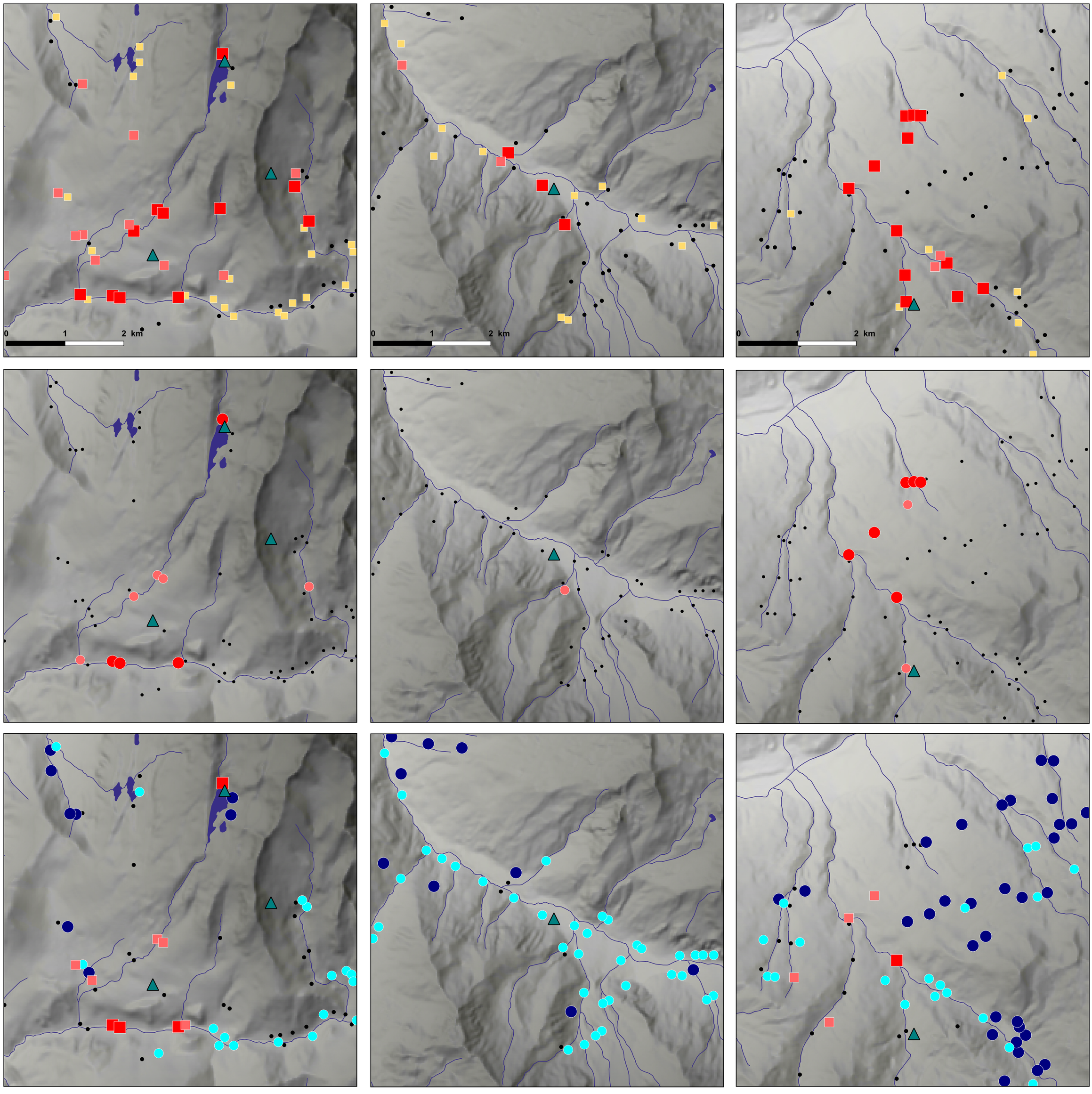

EDA (zPb)
- Other samples (< 4.03)
- High background (4.03 - 7.56)
- Near high outliers (7.56 - 14.17)
- Far high outliers (> 14.17)

Fractal
- Other samples
- High anomaly
- Very high anomaly

Quality/SQI
- Poor (0-45)
- Marginal (45-60)
- Fair (60-80
- Good (80-95)
- Excellent (95-100)

Table 1.

	Fe2O3	MnO	As	Cd	Cr	Cu	Ni	Pb	Zn
	%	%	$mg.kg^{-1}$	$mg.kg^{-1}$	$mg.kg^{-1}$	$mg.kg^{-1}$	$mg.kg^{-1}$	$mg.kg^{-1}$	$mg.kg^{-1}$
Limit of detection	0.1	0.01	20	2	10	10	10	10	10
Min.	<0.1	<0.01	<20	<2	<10	<10	<10	<10	<10
Q1	4.4	0.09	29	<2	45	22	28	32	86
Median (Q2)	5.7	0.13	42	<2	60	32	40	43	112
Mean	5.8	0.16	59	<2	71	39	49	66	138
Q3	7	0.18	62	<2	80	45	55	60	149
Max.	25	2.7	1076	45	1700	1530	1571	8900	8190
Skewness	0.71 (-1.87)	5.07 (-0.11)	5.66 (0.72)	nc	8.98 (0.07)	14.33 (0.05)	11.92 (0.07)	23.93 (1.58)	23.99 (-0.64)
nb. cen (\%)	3 (0.04)	21 (0.3)	942 (13.7)	6411 (93)	56 (0.8)	397 (5.8)	215 (3)	45 (0.7)	93 (1.3)
European topsoils (mean)[1]			11.6	0.28	94.8	17.3	37	32	68.1
TEC [2]			9.79	0.99	43.4	31.6	22.7	35.8	121
PEC [3]			33	4.98	111	149	48.6	128	459

[1] Kabata-Pendias (2011)

[2] MacDonald et al. (2000)

[3] MacDonald et al. (2000)

Table 2.

Categories	**zAs**			**zCu**			**zNi**			**zPb**			**zZn**		
	Cut level	*n*	%	Cut level	*n*	%	Cut level	*n*	%	Cut level	*n*	%	Cut level	*n*	%
Far low outliers	< 0.51	0	0.0	< 0.48	0	0	< 0.64	0	0	< 0.75	0	0	< 0.93	0	0
Near low outliers	0.51 - 1.06	29	0.4	0.48 - 1	2	0.03	0.64 - 1.25	59	0.9	0.75 - 1.41	50	0.7	0.93 - 1.66	170	2.5
Low background	1.06 - 2.21	1711	24.8	1 - 2.11	1764	25.6	1.25 - 2.43	1724	25.0	1.41 - 2.65	1674	24.3	1.66 - 2.98	1570	22.8
Background (Q1-Q3)	2.21 - 3.6	**3439**	49.9	2.11 - 3.46	**3448**	50.0	2.43 - 3.79	**3394**	49.2	2.65 - 4.03	**3459**	50.2	2.98 - 4.39	**3442**	49.9
High background	3.6 - 7.49	1354	19.6	3.46 - 7.26	1516	22.0	3.79 - 7.39	1507	21.9	4.03 - 7.56	1361	19.7	4.39 - 7.84	1407	20.4
Near high outliers	7.49 - 15.59	298	4.3	7.26 - 15.25	139	2.0	7.39 - 14.41	164	2.4	7.56 - 14.17	231	3.4	7.84 - 14.03	236	3.4
Far high outliers	> 15.59	61	0.9	> 15.25	23	0.3	> 14.41	44	0.6	> 14.17	117	1.7	> 14.03	67	1.0

Table 3.

						nb. of samples		
As	range	slope	intercept	r-squared	interpretation	Akima	BRGM dataset	%
1	$<$ 25	-1.163	116.79	0.998	Very low background	602	1400	20.3
2	25-32	-1.733	131.62	0.998	Low background	590	776	28.0
3	32-41	-2.327	150.53	1	Low background	1022	1151	
4	41-60	-1.61	119.58	0.993	Background	1494	1738	37.6
5	60-82	-0.824	73.43	0.985	Background	839	852	
6	82-103	-0.136	19.23	0.995	High background	132	309	12.1
7	103-122	-0.063	11.79	0.961	High background	57	151	
8	122-213	-0.033	7.81	0.925	High background	138	284	
9	213-273	-0.009	3.28	0.879	High background	31	88	
10	273-463	-0.004	1.76	0.859	High anomaly	34	108	1.6
11	$>$ 463	-0.002	1.07	0.968	Very high anomaly	5	35	0.5

						nb. of samples		
Cu	range	slope	intercept	r-squared	interpretation	Akima	BRGM dataset	%
1	$<$ 13	-0.774	105.71	0.996	Very low background	212	661	9.6
2	13-19	-1.227	111.83	0.998	Low background	371	684	39.4
3	19-24	-2.328	132.44	0.999	Low background	590	791	
4	24-31	-3.109	151.41	0.999	Low background	1062	1240	
5	31-43	-2.799	138.99	0.978	Background	1616	1635	46.6
6	43-66	-0.765	52.84	0.941	Background	820	1230	
7	66-90	-0.165	15.94	0.955	Background	194	348	
8	90-126	-0.044	5.35	0.902	High background	65	197	2.9
9	$>$ 126	-0.001	0.33	0.649	High anomaly	14	106	1.5

						nb. of samples		
Ni	range	slope	intercept	r-squared	interpretation	Akima	BRGM dataset	%
1	$<$ 15	-0.615	104.91	0.986	Very low background	227	540	7.8
2	15-24	-1.337	115.68	0.995	Low background	604	801	28.4
3	24-33	-2.027	132.05	0.999	Low background	890	1156	
4	33-45	-2.235	138.18	0.999	Background	1326	1672	51.8
5	45-72	-1.083	84.08	0.958	Background	1363	1901	
6	72-125	-0.146	20.32	0.946	High background	372	613	11.4
7	125-256	-0.016	4.97	0.947	High background	100	165	
8	256-325	-0.003	2.12	0.955	High background	13	11	
9	325-372	-0.004	2.17	0.957	High anomaly	8	0	0.4
10	372-694	-0.002	1.41	0.93	High anomaly	28	26	
11	$>$ 694	-3.99E-04	0.5	0.854	Very high anomaly	13	7	0.1

						nb. of samples		
Pb	range	slope	intercept	r-squared	interpretation	Akima	BRGM dataset	%
1	$<$ 20	-0.21	102.46	0.826	Very low background	107	356	5.2
2	20-28	-1.161	122.02	0.974	Low background	458	852	32.3
3	28-37	-2.58	161.26	0.999	Low background	1147	1372	
4	37-55	-2.153	142.9	0.989	Background	1876	2272	48.7
5	55-77	-0.944	77.79	0.969	Background	925	1085	
6	77-162	-0.092	14.39	0.888	High background	363	719	12.8
7	162-369	-0.006	2.11	0.914	High background	56	160	
8	369-890	-2.98E-04	0.35	0.955	High anomaly	7	42	0.6
9	$>$ 890	-8.94E-05	0.17	0.822	Very high anomaly	5	34	0.5

						nb. of samples		
Zn	range	slope	intercept	r-squared	interpretation	Akima	BRGM dataset	%
1	$<$ 21	-0.043	100.2	0.947	Very low background	33	132	3.9
2	21-43	-0.059	100.76	0.89	Very low background	67	137	
3	43-64	-0.257	110.21	0.928	Low background	238	422	22.2
4	64-87	-0.755	142.67	0.988	Low background	855	1108	
5	87-111	-1.204	181.67	0.998	Background	1383	1584	64.6
6	111-218	-0.463	91.6	0.882	Background	2130	2867	
7	218-294	-0.032	11.56	0.966	High background	125	293	7.4
8	294-465	-0.011	5.25	0.893	High background	89	217	
9	465-597	-0.003	1.61	0.968	High anomaly	18	53	0.8
10	$>$ 597	-1.81E-04	0.22	0.975	Very high anomaly	6	79	1.1

Table 4.

Category	Range	Percentage	Nb of samples
Poor	]-1,45]	1.38	95
Marginal	]45,60]	3.93	271
Fair	]60,80]	31.36	2161
Good	]80,95]	39.61	2730
Excellent	]95,100]	23.72	1635